NONLINEAR CONTROL OF A FLEXIBLE AEROELASTIC SYSTEM

Shakir Jiffri[a], Paolo Paoletti[a], John E. Mottershead[a], Jonathan E. Cooper[b]

[a] *Centre for Engineering Dynamics, School of Engineering, The University of Liverpool, Brownlow Hill, Liverpool L69 3GH.*

[b] *Department of Aerospace Engineering, University of Bristol, Queens Building, University Walk, Bristol BS8 1TR.*

Keywords flutter, nonlinear aeroelasticity, feedback linearisation, adaptive feedback linearisation, control, Small Gain Theorem

Abstract Although it is a common practice in the field of Dynamics to treat a system as being linear, the assumption of linearity is only valid in situations where the effect of any nonlinearities is minimal. Significant nonlinear behaviour (such as Limit Cycle Oscillations) has been observed in many practical manifestations of aeroelastic systems, highlighting the need to account for system nonlinearities. A consequence of incorporating nonlinearity into the model is that the application of linear control methods becomes inadequate when the system operates in a substantially nonlinear regime. Thus, the present work addresses both these concerns by applying nonlinear control on an aeroelastic system consisting of a flexible wing with a structural nonlinearity. The Feedback Linearisation method is employed to render the system linear, such that linear control methods are applicable. The utility of the Small Gain Theorem and Adaptive Feedback Linearisation in situations where errors in the parameters describing the nonlinearities are present is demonstrated.

1. INTRODUCTION

The avoidance of flutter still remains a key constraint in the design of all aircraft. In this endeavour, the need to develop models that accurately reproduce physical phenomena is of growing importance; one such phenomenon is nonlinearity. Substantial nonlinear behaviour such as limit cycle oscillations (LCO) have been observed in several aeroelastic systems [1, 2], making evident the need to account for nonlinearity. The present work gains motivation from this need. The situation where a nonlinear limit cycle oscillation (LCO) response is caused by a structural nonlinearity is considered, and means of mitigating such undesirable response are investigated.

The suitability of linear control methods for flutter suppression in aeroelastic systems is clearly dependent on the extent of nonlinearities present in the system. Application of linear control methods on a nonlinear aeroelastic system with hardening stiffness was investigated experimentally by Block and Strganac in [3]. It was found that the effectiveness of linear control is limited to situations where the airspeed is not much higher than the linear flutter speed, where the LCO amplitude is small. For airspeeds substantially higher than the linear flutter speed (where LCO amplitudes are higher) the control becomes unpredictable, and its effectiveness limited.

Ko *et al*. applied feedback linearisation (with and without adaptation) to a 2 - degree of freedom (DOF) rigid aeroelastic system with torsional nonlinearity [4, 5].This work was later implemented experimentally by Platanitis and Strganac [6], with results indicating an improvement in controlled response when using an additional control surface, but only up to moderately high air velocities. Experimental implementation of adaptive feedback linearisation by Strganac *et al*. [7], produced results suggesting that knowledge of the exact nonlinear parameters is critical to the performance of feedback linearisation in the absence of adaptive methods, and that the adaptive controller substantially improves the controlled response. It was also observed in [7] that performing feedback linearisation without adaptation in the presence of parameter errors caused the system to reach non-zero equilibria.

In this paper, feedback linearisation is applied to a flexible wing with a structural nonlinearity. The latter is introduced to the system by coupling a rigid pylon-engine to the wing via a nonlinear hardening torsional spring. An error in the parameter describing the nonlinearity is considered, and initially the Small Gain Theorem is used to impose bounds on the error function such that closed-loop stability will be guaranteed in the absence of adaptive methods. Subsequently, a substantial error in the nonlinear parameter is introduced, and adaptive feedback linearisation is applied. The resulting controlled response is compared with that obtained when standard feedback linearisation is applied.

2. THE AEROSERVOELASTIC MODEL

The governing equation of the aeroservoelastic model takes the usual form [8] given by

$$\mathbf{A}\ddot{\mathbf{q}} + \left(\rho V\mathbf{B} + \mathbf{D}\right)\dot{\mathbf{q}} + \left(\rho V^2\mathbf{C} + \mathbf{E}\right)\mathbf{q} = \mathbf{f}_{ext}\,, \tag{1}$$

where $\mathbf{A}, \mathbf{D}, \mathbf{E}$ are the inertia, structural damping and structural stiffness matrices respectively, $\mathbf{B}, \mathbf{C}$ are the aerodynamic damping and aerodynamic stiffness matrices respectively, and ρ, V are air density and velocity respectively. The vector $\mathbf{q}$ contains generalised co-ordinates describing the motion of the system, whereas the vector $\mathbf{f}_{ext}$ contains externally applied generalised forcing terms, which may consist of control forces. In this work, modified aerodynamic strip theory has been used to compute the lift and pitch moment acting on the wing. An additional unsteady aerodynamic derivative term (appearing in $\mathbf{B}$) is included to account for significant unsteady effects [8]. Aerodynamic forces/moments arising from the pylon-engine have been assumed to be negligible compared to those associated with the wing. Following an assumed-mode-shapes approach [8, 9], the wing has been assumed to consist of two deflection patterns (depicted in Figure 1), the first being a bending mode, and the second a torsional mode. The origin of the co-ordinate system is at the Leading Edge, root of the wing.

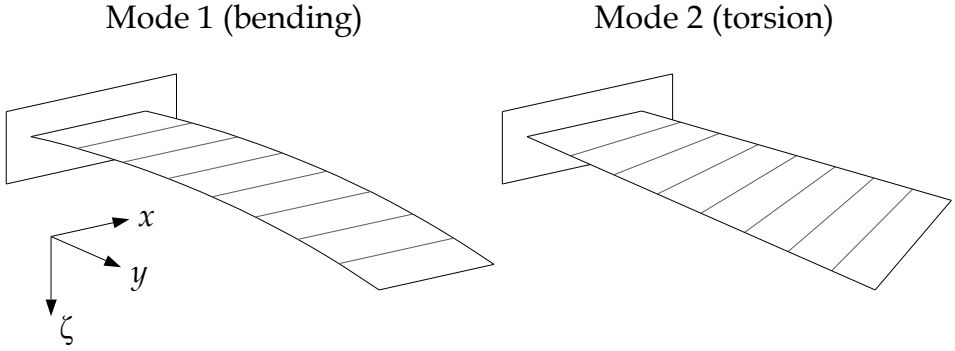

Figure 1 : The two deflection patterns assumed for the flexible wing

Thus, the wing comprises two DOFs. The assumed shapes are incorporated into the wing model by specifying the vertical deflection of the wing ζ at any point (x, y) in terms of contributions from all deflection patterns, viz.,

$$\zeta = y^2 q_1 + y\left(x - x_f\right) q_2\,, \tag{2}$$

where q_1, q_2 are generalised co-ordinates that quantify the amount of bending and torsion modes present in the overall deflection, and x_f is the x- co-ordinate of the wing flexural axis. The pylon-engine depicted in Figure 2 has been modelled as a rigid body, consisting of a solid cylinder (engine) onto which a parallelogram-shaped plate (pylon) has been fixed at the top.

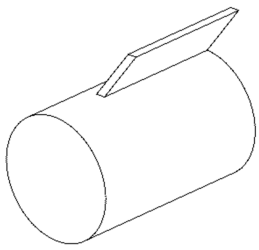

Figure 2 : 3D view of pylon-engine

In this model, the pylon-engine is assumed to have 1 DOF (this brings the dimension of the coupled wing-pylon-engine system to three), which is a rotation about an axis that is parallel to the global *y*-axis, going through the attachment point to the wing (this axis will be referred to as a local *y*-axis). A sketch of the combined wing-pylon-engine is shown in Figure 3.

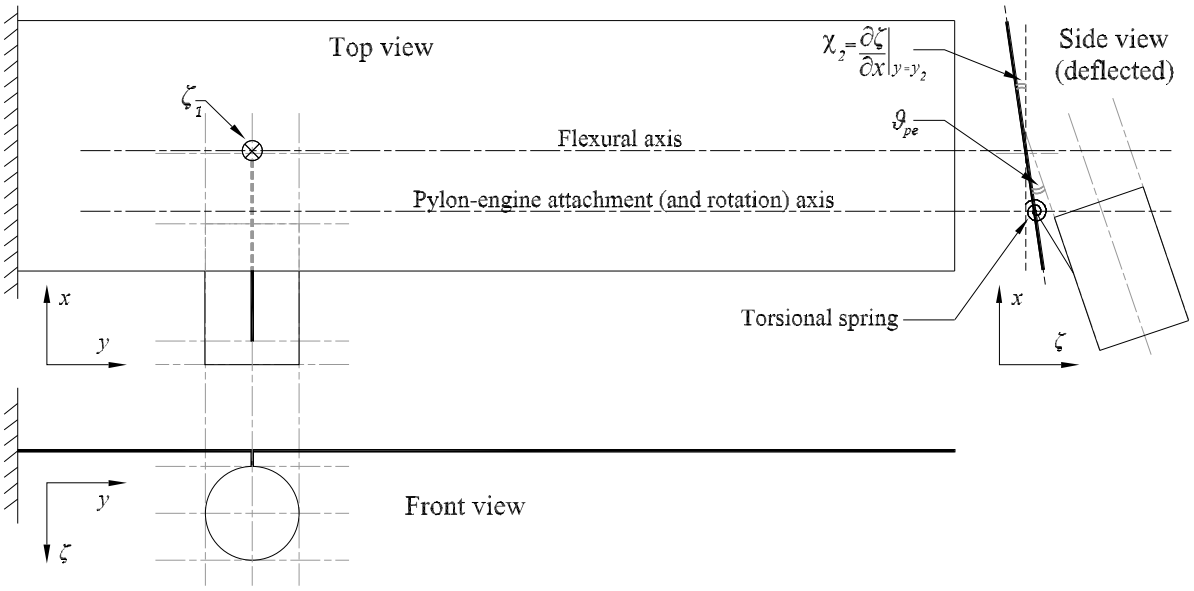

Figure 3 : Various views of the wing- pylon-engine model
(pylon represented by a rigid link, in side view)

Note that ϑ_{pe} is the deflection of the pylon-engine *relative* to the wing. The absolute rotation θ_{pe} may be obtained by adding the wing twist angle at the engine attachment location, χ_2, to ϑ_{pe}. The absolute pylon-engine rotation is also defined in terms of a generalised co-ordinate in the same domain of q_1, q_2 as $\theta_{pe} = \varsigma q_{pe}$, where ς is some arbitrary scalar multiple.

2.1. Co-ordinate Transformation and System Matrices

Since the wing deflection has been defined in assumed-mode-shapes generalised co-ordinates, in order to model the entire wing-pylon-engine system, it is necessary to represent the pylon-engine also in the same domain; this may be achieved by a co-ordinate transformation. A number of physical co-ordinates equal to the number of assumed modes in the system is specified; in the present case, three. One has already been chosen as ϑ_{pe}. The remaining two are chosen as:

a) ζ_1, a vertical deflection at point 1, which lies at the crossing between the wing flexural axis and the local *x*- axis going through the attachment point of the pylon-engine to the wing.
b) χ_2, the wing twist angle at point 2, the pylon-engine attachment location, which is chosen as the intersection of the quarter-semi-span and quarter-chord.

The particular choice of the above two co-ordinates is due to the requirement of these co-ordinates in the derivation of energy expressions for the system. Figure 3 depicts the three physical co-ordinates on the wing-pylon-engine system. Thus, the required transformation takes the form

$$\mathbf{p} = \mathbf{T}\mathbf{q}, \quad \text{where } \mathbf{p} = \left\{\zeta_1 \quad \chi_2 \quad \vartheta_{pe}\right\}^T, \quad \mathbf{q} = \left\{q_1 \quad q_2 \quad q_{pe}\right\}^T, \tag{3}$$

where $\mathbf{T}$ is the equivalence transformation matrix. Using equation (2), $\mathbf{T}$ may be derived as

$$\mathbf{T} = \begin{bmatrix} y_1^2 & 0 & 0 \\ 0 & y_2 & 0 \\ 0 & -y_2 & \varsigma \end{bmatrix}, \tag{4}$$

where y_1, y_2 are the y- co-ordinates at points 1 and 2 respectively. Using the Lagrange equation and aerodynamic strip theory [8], maintaining the same ordering of co-ordinates in equation (3), the system matrices of the wing-pylon-engine system in the assumed-modes domain are derived as

$$\mathbf{A}_{mod} = \begin{bmatrix} m\frac{s_w^5 c_w}{5} + m_{pe}y_1^4 & m\frac{s_w^4}{4}\left(\frac{c_w^2}{2} - c_w x_f\right) & m_{pe}y_1^2 r_G \hat{c}\varsigma \\ m\frac{s_w^4}{4}\left(\frac{c_w^2}{2} - c_w x_f\right) & m\frac{s_w^3}{3}\left(\frac{c_w^3}{3} - c_w^2 x_f + c_w x_f^2\right) & 0 \\ m_{pe}y_1^2 r_G \hat{c}\varsigma & 0 & \left(I_G + m_{pe}r_G^2\right)\varsigma^2 \end{bmatrix}, \tag{5}$$

$$\mathbf{E}_{mod} = \begin{bmatrix} 4EIs_w & 0 & 0 \\ 0 & GJs_w + K_T y_2^2 & -K_T y_2 \varsigma \\ 0 & -K_T y_2 \varsigma & K_T \varsigma^2 \end{bmatrix}, \tag{6}$$

$$\mathbf{B}_{mod} = \begin{bmatrix} \frac{c_w a_W s_w^5}{10} & 0 & 0 \\ -\frac{c_w^2 e a_W s_w^4}{8} & -\frac{c_w^3 s_w^3 M_{\dot{\theta}}}{24} & 0 \\ 0 & 0 & 0 \end{bmatrix}, \quad \mathbf{C}_{mod} = \begin{bmatrix} 0 & \frac{c_w s_w^4 a_W}{8} & 0 \\ 0 & -\frac{e c_w^2 s_w^3 a_W}{6} & 0 \\ 0 & 0 & 0 \end{bmatrix}. \tag{7}$$

In equations (5) and (6), c_w, s_w are the wing chord and semi-span respectively, m the wing mass per unit area, EI, GJ the wing flexural and torsional rigidity respectively, m_{pe} the combined mass of the pylon and engine, I_G the moment of inertia of the pylon-engine referred to a local y-axis going through the pylon-engine centre of mass (COM), $\hat{c}$ the cosine of the angle of the pylon-engine COM relative to the top flat surface of the pylon taken about the flexural axis, r_G the distance between the flexural axis and the local y- axis mentioned above, and K_T the linear torsional coupling stiffness of the spring connecting the pylon-engine to the wing. In equation (7) the eccentricity ratio e is the distance between the aerodynamic centre and flexural axis as a

fraction of the chord, a_W is the lift curve slope and $M_{\dot{\theta}}$ the non-dimensional pitch damping derivative. As it has been assumed that the pylon-engine does not participate in the aerodynamics, the corresponding terms in $\mathbf{B}_{mod}, \mathbf{C}_{mod}$ are zero. An appropriate level of structural damping $\mathbf{D}_{mod}$ may be included in the model. A convenient way of doing this is to specify the damping in the modal domain [10], and subsequently transforming into the assumed-modes domain using the eigenvectors of the undamped system.

2.2. Forcing Terms

The aileron (control surface) usually provides the necessary means to apply control forces to the wing-pylon-engine system. It is assumed in this work that two control surfaces are available, the first (closest to the wing root) spanning 85% of the length of the wing and the second spanning the remaining length (the contribution of the control surfaces to the dynamics of the overall system is neglected). The widths of the first and second control surfaces are set at 20% and 33.33% of the chord length respectively, so as to optimise the distribution of work performed by each control surface. It is also assumed that a separate actuator is available to apply a torque T_{pe} directly on the engine rotational DOF. Again, using the Lagrange equation and aerodynamic strip theory, the forcing vector is found as

$$\mathbf{f}_{c,mod} = \begin{bmatrix} -\frac{1}{6}\tilde{r}\alpha^3 a_{C,1} s_w & -\frac{1}{6}\tilde{r}\left(1-\alpha^3\right) a_{C,2} s_w & 0 \\ \frac{1}{4}\tilde{r}\alpha^2 b_{C,1} c_w & \frac{1}{4}\tilde{r}\left(1-\alpha^2\right) b_{C,2} c_w & -y_2 \\ 0 & 0 & \varsigma \end{bmatrix} \begin{Bmatrix} \beta_1 \\ \beta_2 \\ T_{pe} \end{Bmatrix} =: \bar{\mathbf{B}}_{mod}\mathbf{u}, \quad \begin{matrix} \tilde{r} := \rho V^2 c_w s_w^2, \\ \alpha = 0.85 \end{matrix} \tag{8}$$

and each surface will have its own deflection angle β_1, β_2 and set of aerodynamic parameters a_C, b_C [11], which are the rates of change of lift coefficient and moment coefficient respectively, with respect to control surface deflection angle.

2.3. Inclusion of Nonlinearity

The nonlinear force may be incorporated as an internal force in the equation of motion, viz.,

$$\mathbf{A}_{mod}\ddot{\mathbf{q}} + \left(\rho V \mathbf{B}_{mod} + \mathbf{D}_{mod}\right)\dot{\mathbf{q}} + \left(\rho V^2 \mathbf{C}_{mod} + \mathbf{E}_{mod}\right)\mathbf{q} + \mathbf{f}_{nl,mod} = \mathbf{f}_{c,mod}, \tag{9}$$

expressed in the assumed-modes domain. In the present model, a cubic hardening nonlinearity is assumed in the torsional spring connecting the pylon-engine to the wing. The nonlinear force in the spring is expressed as $K_{T,nl}\vartheta_{pe}^3$, where $K_{T,nl}$ is the cubic stiffness coefficient. Since ϑ_{pe} is a relative deflection (involving both coupling DOFs), the nonlinear force vector takes the form

$$\mathbf{f}_{nl,mod} = \mathbf{T}^T \mathbf{f}_{nl}, \quad \text{where } \mathbf{f}_{nl} = \begin{Bmatrix} 0 & 0 & K_{T,nl}\vartheta_{pe}^3 \end{Bmatrix}^T, \tag{10}$$

with $\mathbf{T}$ defined in equation (4).

3. NUMERICAL SIMULATION – UNCONTROLLED SYSTEM

A numerical simulation of the aeroelastic model is now performed. Initially, dimensions and parameters for the wing and pylon-engine are chosen. A frequency domain computation is then performed on the linear system, and thereby the linear flutter speed is determined. Subsequently, a cubic hardening stiffness is included in the torsional spring connecting the wing to the pylon-

engine, and the nonlinear time-domain response is simulated above the flutter speed. It is assumed that there is no external excitation, but that there is an initial deflection.

3.1. Model Dimensions and Parameters

The dimensions and parameters chosen for the model are given in Table 1 and Table 2. For the flexible wing, the values chosen are based on those used in a numerical example found in [8]. The dimensions and mass of the pylon-engine have been chosen such that their proportion with respect to those of the wing is similar to what one might find in a real aircraft (e.g. [12]).

Semi-span (s_w)	7.5 m	Flexural rigidity (EI)	3,675	Eccentricity ratio (e)	0.23
Chord (c_w)	2.0 m	Torsional rigidity	1,890		
Flexural axis (x_f)	0.96 m	Air density (ρ)	1.225 kgm^{-3}	Non-dimensional pitch damping derivative ($M_{\dot{\theta}}$)	-1.2
Mass/unit area (m)	100 kgm^{-2}	Lift curve slope (a_W)	2π		

Table 1 : Dimensions and Parameters of Flexible Wing

Engine diameter (d_e)	0.75	Engine mass (m_e)	350 kg	Engine length (l_e)	1.125
Pylon mass (m_p)		35 kg	Pylon height (h_p)		0.125
Coupling torsional spring stiffness (K_T)		511 kNm/rad	Coefficient of cubic component of coupling stiffness ($K_{T,nl}$)		$300K_T$

Table 2 : Dimensions and Parameters of Pylon-Engine

3.2. Airspeed vs. Natural Frequency and Airspeed vs. Damping Ratio Plots

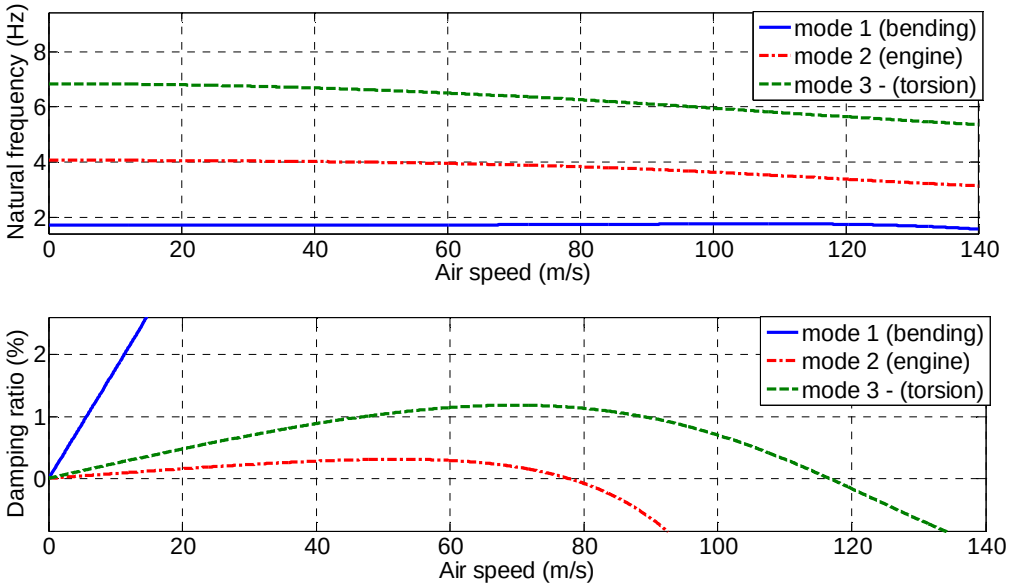

Figure 4 : V-omega and V-zeta plots for the wing-pylon-engine model

The structural modes in the combined model occur at 1.71 Hz (bending), 4.06 Hz (pylon-engine mode) and 6.83 Hz (torsional). It is evident from Figure 4 that flutter initially occurs at an airspeed of 77.6 ms^{-1}, involving coupling of the pylon-engine mode and wing bending modes.

3.3. Nonlinear Time-domain Response

The nonlinear system is simulated at an airspeed of 80 ms^{-1}, just above the flutter point, under the application of the initial conditions ζ_1 = 0.333 mm, χ_2 = 0.00333 rad, ϑ_{pe} = 0.05 rad. These values have been chosen as they are representative of typical physical displacements one might expect in practice, for a wing-pylon-engine system having the dimensions and parameters specified in Table 1 and Table 2 above. The resulting response of the system clearly exhibits LCO. A sample of the response for the ϑ_{pe} co-ordinate is shown in Figure 5.

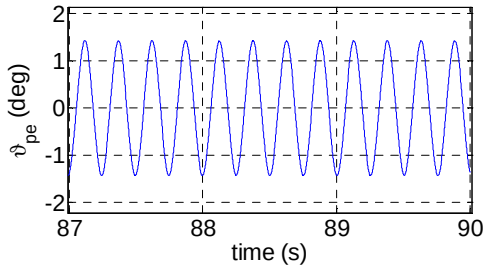

Figure 5 : Steady-state LCO in ϑ_{pe} response

For comparison, when the response for the ϑ_{pe} co-ordinate just below the linear flutter speed is simulated, as expected the response continues to decay, and converges to the origin.

4. LINEARISED CLOSED-LOOP SYSTEM USING NONLINEAR CONTROL

Feedback linearisation [13] is a process applied to a nonlinear system $\dot{\mathbf{x}} = \underline{\mathbf{f}}(\mathbf{x}) + \underline{\mathbf{G}}(\mathbf{x})\mathbf{u}$ to transform it into a linear system $\mathbf{z} = \underline{\mathbf{A}}\mathbf{z} + \underline{\mathbf{B}}\bar{\mathbf{u}}$, based on a particular choice of output $\mathbf{y} = \mathbf{h}(\mathbf{x})$. In these equations $\mathbf{u}$, $\bar{\mathbf{u}}$ are the inputs to the nonlinear and linear systems respectively. The mapping from the nonlinear domain to the linear domain is achieved through a non-singular co-ordinate transformation $\mathbf{z} = \mathbf{T}_{\mathbf{zx}}(\mathbf{x})$. A mapping between $\mathbf{u}$, $\bar{\mathbf{u}}$ is also required.

The present work assumes the use of 3 inputs and 3 outputs. Since the number of outputs is equal to the dimension of the system, the entire nonlinear system is linearised; thus, the complete dynamics of the original system are preserved. Feedback linearisation is applied to the nonlinear model developed above. It is appropriate to use the assumed-modes representation of the system matrices because once the system has been linearised, pole-placement may be performed directly on the assumed modes to shift their respective poles to more desirable locations.

4.1. Nonlinear State-Space Model and Linearising Feedback

Substituting from equation (8) into equation (9), the system is expressed in state-space form as

$$\dot{\mathbf{x}} = \underline{\mathbf{f}}(\mathbf{x}) + \underline{\mathbf{G}}(\mathbf{x})\mathbf{u}, \quad \text{with } \mathbf{x} =: \begin{Bmatrix}\mathbf{q}\\ \mathbf{v}\end{Bmatrix}, \quad \mathbf{q} =: \{x_1 \quad x_2 \quad x_3\}^T, \quad \mathbf{v} =: \{x_4 \quad x_5 \quad x_6\}^T, \quad (11)$$

where

$$\underline{\mathbf{f}}(\mathbf{x}) = \begin{Bmatrix} \mathbf{v} \\ \boldsymbol{\Psi}\mathbf{q} + \boldsymbol{\Phi}\mathbf{v} + \boldsymbol{\Omega}\mathbf{f}_{nl,\,mod} \end{Bmatrix}, \quad \underline{\mathbf{G}}(\mathbf{x}) = \begin{bmatrix} \mathbf{0} \\ \boldsymbol{\Xi} \end{bmatrix}, \tag{12}$$

and

$$\begin{gathered} \boldsymbol{\Psi} := -\mathbf{A}_{mod}^{-1}\left(\rho V^2 \mathbf{C}_{mod} + \mathbf{E}_{mod}\right), \quad \boldsymbol{\Phi} := -\mathbf{A}_{mod}^{-1}\left(\rho V \mathbf{B}_{mod} + \mathbf{D}_{mod}\right), \\ \boldsymbol{\Omega} := -\mathbf{A}_{mod}^{-1}, \quad \boldsymbol{\Xi} := \mathbf{A}_{mod}^{-1}\bar{\mathbf{B}}_{mod}\,. \end{gathered} \tag{13}$$

The inputs (defined in section 2.2) and outputs respectively are chosen as

$$\mathbf{u} = \begin{Bmatrix} \beta_1 & \beta_2 & T_{pe} \end{Bmatrix}^T, \quad \mathbf{y} = \begin{Bmatrix} y_a & y_b & y_c \end{Bmatrix}^T := \begin{Bmatrix} q_1 & q_2 & q_{pe} \end{Bmatrix}^T = \begin{Bmatrix} x_1 & x_2 & x_3 \end{Bmatrix}^T, \tag{14}$$

thus, it is desired to control all three motions of the system using all three available inputs. Now, following the procedure of Input-Output feedback linearisation [13], the outputs are differentiated with respect to time, whilst substituting for $\dot{\mathbf{x}}$ from equation (11) at each stage. This results in

$$\begin{gathered} \dot{y}_a = x_4, \qquad \dot{y}_b = x_5, \qquad \dot{y}_c = x_6, \\ \ddot{y}_a = f_4 + \begin{bmatrix} g_{41} & g_{42} & g_{43} \end{bmatrix}\mathbf{u}, \quad \ddot{y}_b = f_5 + \begin{bmatrix} g_{51} & g_{52} & g_{53} \end{bmatrix}\mathbf{u}, \quad \ddot{y}_c = f_6 + \begin{bmatrix} g_{61} & g_{62} & g_{63} \end{bmatrix}\mathbf{u}, \end{gathered} \tag{15}$$

where f_i denotes the i^{th} term of the vector $\underline{\mathbf{f}}(\mathbf{x})$, and g_{ij} denotes the ij^{th} term of the matrix $\underline{\mathbf{G}}(\mathbf{x})$. A new co-ordinate system is now defined, which will provide a mapping from the equivalent linear system that is sought, to the original nonlinear system. Using equations (11) and (14), the co-ordinates corresponding to the linearised system are defined as

$$\begin{aligned} z_1 &:= y_a = q_1 = x_1, & z_2 &:= \dot{y}_a = \dot{q}_1 = \dot{x}_1 = x_4, \\ z_3 &:= y_b = q_2 = x_2, & z_4 &:= \dot{y}_b = \dot{q}_2 = \dot{x}_2 = x_5, \\ z_5 &:= y_c = q_{pe} = x_3, & z_6 &:= \dot{y}_c = \dot{q}_{pe} = \dot{x}_3 = x_6. \end{aligned} \tag{16}$$

The above expressions provide the required co-ordinate transformation, which evidently is a permutation of the identity matrix. Note that this non-singular transformation is independent of $\mathbf{x}$, and is therefore globally valid. Now, the vector of actual inputs may be chosen so as to cancel the nonlinearity in the controlled system, viz.,

$$\mathbf{u} = \boldsymbol{\Xi}^{-1}\left(\bar{\mathbf{u}} - \underline{\mathbf{f}}(\mathbf{x})_{([4,5,6],1)}\right), \tag{17}$$

where $\underline{\mathbf{f}}(\mathbf{x})_{([4,5,6],1)}$ contains the 4th, 5th and 6th rows of $\underline{\mathbf{f}}(\mathbf{x})$ in equation (11), i.e.

$$\underline{\mathbf{f}}(\mathbf{x})_{([4,5,6],1)} = \boldsymbol{\Psi}\mathbf{q} + \boldsymbol{\Phi}\mathbf{v} + \boldsymbol{\Omega}\mathbf{f}_{nl,\,mod}, \tag{18}$$

from equation (12). It may be shown that for this choice of inputs, the state-space equations $\dot{\mathbf{z}} = \underline{\mathbf{A}}\mathbf{z} + \underline{\mathbf{B}}\bar{\mathbf{u}}$ decouple to provide the following three controlled single-DOF systems:

$$\begin{Bmatrix} \dot{z}_1 \\ \dot{z}_2 \end{Bmatrix} = \begin{bmatrix} 0 & 1 \\ 0 & 0 \end{bmatrix}\begin{Bmatrix} z_1 \\ z_2 \end{Bmatrix} + \begin{bmatrix} 0 \\ 1 \end{bmatrix}\bar{u}_1, \quad \begin{Bmatrix} \dot{z}_3 \\ \dot{z}_4 \end{Bmatrix} = \begin{bmatrix} 0 & 1 \\ 0 & 0 \end{bmatrix}\begin{Bmatrix} z_3 \\ z_4 \end{Bmatrix} + \begin{bmatrix} 0 \\ 1 \end{bmatrix}\bar{u}_2, \quad \begin{Bmatrix} \dot{z}_5 \\ \dot{z}_6 \end{Bmatrix} = \begin{bmatrix} 0 & 1 \\ 0 & 0 \end{bmatrix}\begin{Bmatrix} z_5 \\ z_6 \end{Bmatrix} + \begin{bmatrix} 0 \\ 1 \end{bmatrix}\bar{u}_3, \tag{19}$$

where $\bar{\mathbf{u}} =: \{\bar{u}_1 \quad \bar{u}_2 \quad \bar{u}_3\}^T$ is the vector of inputs to the linear system. Note that the above three single-DOF systems correspond to the assumed-modes generalised co-ordinates q_1, q_2, q_{pe} respectively (see equation (16)). The artificial inputs may be chosen as a linear combination of instantaneous displacement and velocity, so as to modify the natural frequency and damping ratio of each of these systems respectively, viz.,

$$\bar{u}_1 = -\begin{bmatrix} \bar{f}_1 & \bar{g}_1 \end{bmatrix} \begin{Bmatrix} z_1 \\ z_2 \end{Bmatrix}, \qquad \bar{u}_2 = -\begin{bmatrix} \bar{f}_2 & \bar{g}_2 \end{bmatrix} \begin{Bmatrix} z_3 \\ z_4 \end{Bmatrix}, \qquad \bar{u}_3 = -\begin{bmatrix} \bar{f}_3 & \bar{g}_3 \end{bmatrix} \begin{Bmatrix} z_5 \\ z_6 \end{Bmatrix}. \tag{20}$$

5. TREATMENT OF NONLINEAR PARAMETER ERROR

It is of interest to study the effect of a nonlinear parameter error on the performance of the closed-loop system. The error in the parameter results in an error in $\mathbf{f}_{nl,\,mod}$ which, using equation (10) and the definition of $\mathbf{s}$ from the previous section, may be defined as

$$\boldsymbol{\varepsilon} = \left(\mathbf{f}_{nl,\,mod} - \mathbf{f}'_{nl,\,mod}\right) =: \left(K_{T,\,nl} - K'_{T,\,nl}\right)\vartheta_{pe}^3 \mathbf{s} =: \tilde{K}_{T,\,nl}\vartheta_{pe}^3 \mathbf{s}, \quad \text{where } \mathbf{s}^T = \mathbf{T}_{(3,:)}, \tag{21}$$

$\mathbf{f}'_{nl,\,mod}$ is the nonlinear force vector based on the erroneous value $K'_{T,\,nl}$ of the nonlinear parameter, and $\tilde{K}_{T,\,nl}$ is the error. In the presence of error, the nonlinearity on which the linearising feedback is based takes on the erroneous value. Thus, the input (equation (17)) becomes

$$\mathbf{u} = \boldsymbol{\Xi}^{-1}\left(\bar{\mathbf{u}} - \underline{\mathbf{f}}'(\mathbf{x})_{([4,5,6],1)}\right), \quad \text{where} \quad \underline{\mathbf{f}}'(\mathbf{x})_{([4,5,6],1)} := \boldsymbol{\Psi}\mathbf{q} + \boldsymbol{\Phi}\mathbf{v} + \boldsymbol{\Omega}\mathbf{f}'_{nl,\,mod}. \tag{22}$$

Combining equations (21), (22) and (11), it can be shown that

$$\dot{\mathbf{q}} = \mathbf{v}, \qquad \dot{\mathbf{v}} = \bar{\mathbf{u}} + \boldsymbol{\Omega}\boldsymbol{\varepsilon}. \tag{23}$$

Similar to equation (20), one may express $\bar{\mathbf{u}}$ as a linear transformation of $\mathbf{x}$, viz.,

$$\bar{\mathbf{u}} = \mathbf{G}_{\mathbf{x}}\mathbf{x} = \mathbf{G}_{\mathbf{q}}\mathbf{q} + \mathbf{G}_{\mathbf{v}}\mathbf{v}. \tag{24}$$

Combining the above expression with equation (23), along with the definition of the output,

$$\dot{\mathbf{x}} = \mathbf{A}_{cl,x}\mathbf{x} + \mathbf{B}_x\hat{\mathbf{u}}, \qquad \hat{y} = \mathbf{C}_x\mathbf{x}, \qquad \text{where} \quad \hat{\mathbf{u}} = \boldsymbol{\varepsilon}, \quad \hat{y} = \vartheta_{pe}, \tag{25}$$

and

$$\mathbf{A}_{cl,x} = \begin{bmatrix} \mathbf{0} & \mathbf{I} \\ \mathbf{G}_{\mathbf{q}} & \mathbf{G}_{\mathbf{v}} \end{bmatrix}, \qquad \mathbf{B}_x = \begin{bmatrix} \mathbf{0} \\ \boldsymbol{\Omega} \end{bmatrix}, \qquad \mathbf{C}_x = \mathbf{s}^T\begin{bmatrix} \mathbf{I} & \mathbf{0} \end{bmatrix}. \tag{26}$$

Thus, equation (25) shows how the nonlinear parameter error results in an input to the closed-loop system. Note that the output defined here is different from that defined for the purpose of linearising the system. The effect of the error input on this output may be quantified by the gain of the above system. Commonly used measures for the gain of systems of the form being considered here are the H_∞ and L_1 norms [14, 15], which may be readily computed using the matrices in equation (26). In the case of the L_1 norm, it is usual to use the so-called H* norm, an upper-bound on the L_1 norm, owing to the computational complexity associated with finding the latter [16].

5.1. Imposing bounds on error input parameters – Small Gain Theorem

Having computed the above norms, the Small Gain Theorem [14] may be used to impose bounds on the variables that the error input $\boldsymbol{\varepsilon}$ depends on. The theorem states that for guaranteed input-output stability of two interconnected feedback systems with gains γ_1, γ_2, it is required that $\gamma_1 \gamma_2 < 1$. In the present case, the two systems are (a) the closed-loop system in equation (25), and (b) the relationship between $\boldsymbol{\varepsilon}$ and the nonlinear parameter $\tilde{K}_{T,nl}$. A Lipschitz constant [14] may be used to compute an upper bound for the gain of the error function $\boldsymbol{\varepsilon}$ with respect to its input ϑ_{pe}. An expression for the gain of the error function may be computed as a local Lipschitz constant $\tilde{\beta}$, as

$$\tilde{\beta} = \sup_{|\vartheta_{pe}| < |\vartheta_{pe}|_{max}} \left| \frac{d\boldsymbol{\varepsilon}}{d\vartheta_{pe}} \right| = 3\tilde{K}_{T,nl} \left| \vartheta_{pe} \right|^2_{max} |\mathbf{s}| . \tag{27}$$

Combining the estimate of the L_1 norm computed earlier with the above equation, an amplitude bound $|\vartheta_{pe}|$ that satisifies the Small Gain Theorem is computed as

$$|\vartheta_{pe}|_{max} = \sqrt{\frac{1}{3\tilde{K}_{T,nl}\gamma_* |\mathbf{s}|}} . \tag{28}$$

It should be noted that the bounds computed using the H_∞ and H* norms are conservative, as is the Small Gain Theorem. Thus, it may be possible to exceed the bounds computed by this approach and yet have a stable closed-loop system, although stability beyond these bounds cannot be guaranteed.

6. ADAPTIVE FEEDBACK LINEARISATION

It was described in the above section how a discrepancy between the actual nonlinearity and assumed nonlinearity used in the linearising feedback acts as an input to the closed-loop system. It is possible that this additional (unknown) input may destabilise the system - or at least degrade control performance – if its magnitude exceeds the bounds computed, for example, by the approach discussed in section 5.1. This possibility may be eliminated by accounting for nonlinearity errors using an adaptive scheme. Such a scheme will guarantee asymptotic stability of the closed-loop response. Essentially, the adaptive scheme entails continuously updating the assumed value of the nonlinear parameter, such that a positive scalar Lyapunov function based on the state and parameter error is continuously decreasing. Thus, a parameter update rate satisfying this requirement may be computed, such that closed-loop stability is ensured.

7. NUMERICAL SIMULATION – CLOSED LOOP SYSTEM

Closed-loop control is applied to the nonlinear model in the assumed-modes domain to provide linearising feedback. The latter is computed such that the linearised system consists of the uncoupled SDOF sub-systems referred to earlier. The following modal parameters are set for pole-placement of the system at 80 ms^{-1}:

q_1	0.93 Hz	0.01	q_2	4.95 Hz	0.01	q_{pe}	2.9 Hz	0.01

The values specified above are in the same order of magnitude as the bending, torsional and pylon-engine mode natural frequencies (see Figure 4). The initial conditions are set at the same values used in the uncontrolled case (section 3.3), namely ζ_1 = 0.333 mm, χ_2 = 0.00333 rad, ϑ_{pe} = 0.05 rad.

In the absence of any nonlinear parameter error, as one would expect, the controlled assumed-modes are modified such that their natural frequencies and damping ratios are identical to those in the above table and the impulse response decays to zero, as seen in Figure 6.

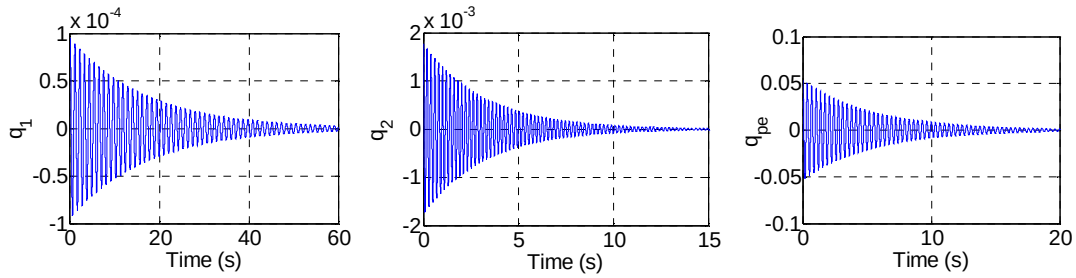

Figure 6 – Feedback-linearised response at 80 ms^{-1} (assumed-modes co-ordinates)

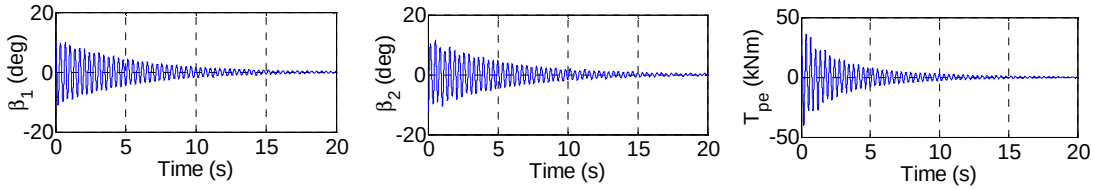

Figure 7 : Control surface deflection angles and actuator torques for exact feedback linearisation

The required control surface and actuator inputs are shown in Figure 7, where it can be seen that the input magnitudes are feasible in practice. When a 40% error in $K_{T,nl}$ is incorporated, and the closed-loop response is simulated based on the above feedback parameters and with the same initial conditions, an unstable response sets in from the very beginning, as seen in Figure 8.

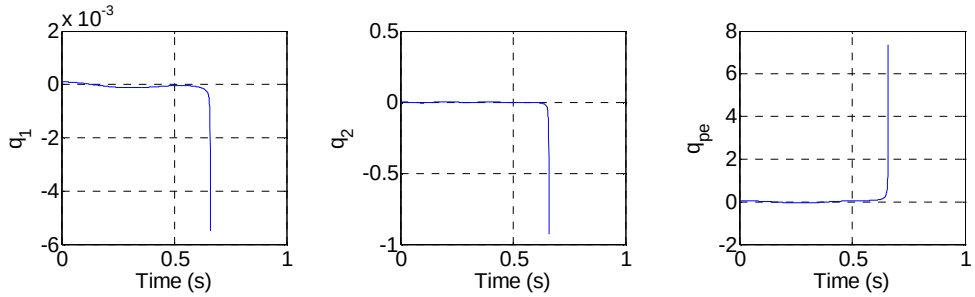

Figure 8 : Feedback-linearised response at 80 ms^{-1}, with nonlinear parameter error included

At this point, it is appropriate to compute an estimate of the bounds on the error function (see equation (21)) using the approach discussed in section 5 above. The matrices in the state-space equation (25) are assembled, and the H_∞ and H* norms are subsequently computed. For the H* problem, μ, λ are chosen as 0.003 and 0.115 respectively. The Yalmip and Sedumi Matlab toolboxes [17, 18] have been used to solve the LMIs. Having computed the norms γ_∞ and γ_*, which are 2.4×10^{-4} and 4.25×10^{-4} respectively, the Small Gain Theorem is used to compute appropriate bounds in each case. Suppose it is desired to keep the estimated error in $K_{T,nl}$ at 40%. In this case, the bound should be imposed on the allowable deflection angle ϑ_{pe}. Using equation (28), the allowable magnitudes in the H_∞ and H* cases are computed as 0.003265 and 0.002453 radians respectively. Given that ϑ_{pe} is being controlled such that the amplitude of its vibration envelope is decreasing, its initial value may be set to the maximum allowable bound computed above (thus, it is ensured that the magnitude of ϑ_{pe} will not exceed the allowable

bound). When the simulation is repeated with the initial condition of ϑ_{pe} set to the H_∞ bound 0.003265 for example, it is seen that the resulting response is stable. In fact, instability only begins when ϑ_{pe} is approximately 0.043 rad.

The instability shown in Figure 8 may be avoided altogether by implementing the adaptive controller described in section 6 above. In this case, the resulting controlled response, again for the same initial conditions, is shown in Figure 9.

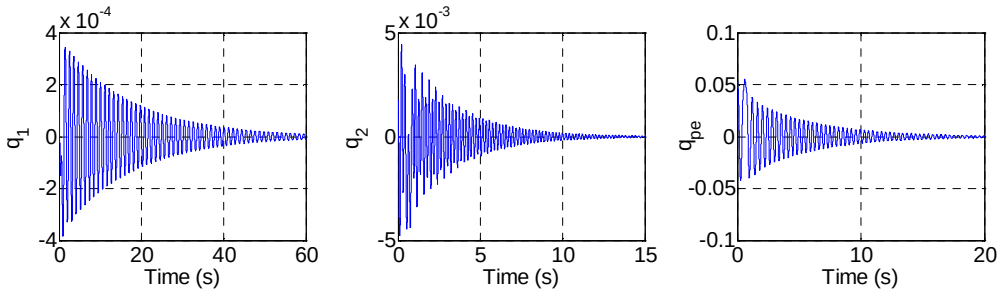

Figure 9 : Feedback-linearised response at 80 ms^{-1}, with parameter adaptation

A comparison between Figure 9 and Figure 6 shows that the controlled responses are similar, but not identical. Although the original pole-placement requirement has not been satisfied, it can be seen that the controlled response is stable. Note that by implementing the adaptive controller, it has been possible to significantly exceed the bounds on $|\vartheta_{pe}|$ as estimated by the Small Gain Theorem. In fact, the adaptive controller successfully drives the responses to zero for values of $|\vartheta_{pe}|_{max}$ (set as an initial condition) up to around 0.0735 rad. The required control in this case is accomplished through achievable control surface deflection angles (≈11˚) and actuator torque magnitude (55 kNm).

8. CONCLUSIONS

This work demonstrates the application of adaptive feedback linearisation on a 3-DOF flexible aeroelastic model consisting of a flexible wing and a rigid pylon-engine attached to the wing by a nonlinear torsional spring. For the dimensions and parameters chosen in the illustrations, the initial flutter is caused by the pylon-engine mode, which is a novel contribution of this paper.

The availability of 3 inputs and 3 outputs is assumed in the feedback linearisation of the 3-DOF aeroelastic system. The inputs are provided by two ailerons and a torsional actuator, and the outputs measured are the wing bending and torsional displacements, and relative angular deflection between wing and pylon-engine. This configuration is advantageous as it leads to a completely linearised system, enabling control of all 3 co-ordinates of the system. Pole-placement through linearising feedback is achieved successfully in the absence of nonlinear parameter error, which is expected. When a sizeable error in the nonlinear parameter is introduced, an unstable response is encountered immediately. The Small Gain Theorem is applied to estimate bounds on acceptable error magnitudes to ensure stable controlled response in the absence of adaptive methods. The estimated L_1 gain provides a reasonable estimate of the allowable pylon-engine deflection for a fixed (estimate of) nonlinear parameter error.

Application of adaptive feedback linearisation leads to a marked improvement in controlled response by preventing the instability previously seen, and causes the response to converge to the origin. Numerical simulations confirm this fact, revealing that stabilising adaptive control can be implemented with achievable magnitudes of aileron deflection angles. This result is compared

with the closed-loop response obtained when nonlinearity errors are ignored during feedback linearisation; a marked improvement in response is observed when adaptation is included.

In work that is due to appear elsewhere, the authors of this paper present a new treatment of the application of Feedback Linearisation to general second-order systems [19], in a second-order representation that is familiar in the area of elasto-mechanics and aeroelasticty.

ACKNOWLEDGEMENTS

This research has been funded by EPSRC grant EP/J004987/1 under the project entitled "Nonlinear Active Vibration Suppression in Aeroelasticity".

9. REFERENCES

[1] Dowell E., Edwards J., Strganac T., *Nonlinear aeroelasticity.* Journal of Aircraft, 2003. **40**(5): pp. 857-874
[2] Lee B.H.K., Price S.J., Wong Y.S., *Nonlinear aeroelastic analysis of airfoils: bifurcation and chaos.* Progress in Aerospace Sciences, 1999. **35**(3): pp. 205-334
[3] Block J.J., Strganac T.W., *Applied active control for a nonlinear aeroelastic structure.* Journal of Guidance Control and Dynamics, 1998. **21**(6): pp. 838-845
[4] Ko J., Kurdila A.J., Strganac T.W., *Nonlinear control of a prototypical wing section with torsional nonlinearity.* Journal of Guidance Control and Dynamics, 1997. **20**(6): pp. 1181-1189
[5] Ko J., Kurdila A.J., Strganac T., *Stability and control of a structurally nonlinear aeroelastic system.* Journal of Guidance Control and Dynamics, 1998. **21**: pp. 718-725
[6] Platanitis G., Strganac T.W., *Control of a nonlinear wing section using leading- and trailing-edge surfaces.* Journal of Guidance Control and Dynamics, 2004. **27**(1): pp. 52-58
[7] Strganac T., Ko J., Thompson D., *Identification and control of limit cycle oscillations in aeroelastic systems.* Journal of Guidance Control and Dynamics, 2000. **23**(6): pp. 1127-1133
[8] Wright J.R., Cooper J.E., *Introduction to Aircraft Aeroelasticity and Loads*. 2007, Chichester: Wiley.
[9] Meirovitch L., *Analytical Methods in Vibrations*. 1967, New York: Macmillan USA.
[10] Rao S.S., *Mechanical Vibrations*. 4th ed. 2004: Prentice Hall.
[11] Fung Y.C., *An Introduction to the Theory of Aeroelasticity*. 1969: Dover.
[12] http://www.airbus.com/aircraftfamilies/passengeraircraft/a330family/a330-200/specifications/, Last accessed 04.04.2013
[13] Isidori A., *Nonlinear Control Systems*. 1995, Berlin Heidelberg New York: Springer.
[14] Khalil H.K., *Nonlinear Systems*. 3rd ed. 2002: Prentice Hall.
[15] Scherer C., Weiland S., *Linear Matrix Inequalities in Control.* Dutch Institute of Systems and Control course notes, 2000
[16] Dahleh M.A., Pearson J.B., *L1-Optimal Compensators for Continuous-time Systems.* IEEE Transactions on Automatic Control, 1987. **32**(10): pp. 889-895
[17] http://users.isy.liu.se/johanl/yalmip/pmwiki.php?n=Main.Download, Last accessed 02.04.13
[18] http://sedumi.ie.lehigh.edu/, Last accessed 02.04.13
[19] Jiffri S., Paoletti P., Cooper J.E., Mottershead J.E., *Feedback Linearisation for Nonlinear Vibration Control.* Journal of Sound and Vibration, Submitted 2013